Stress and dislocations in thin metal layers

Nicola, Lucia

Chapter 6

Effect of defect energy on strain gradient predictions of confined plasticity*

In the previous chapters it is shown that the discrete dislocation plasticity framework is suitable of capturing size effects in thin films under tension. In work, for example, by Cleveringa et al. [1] a size dependent response is found for other small structures, including composite materials with specific particle shapes [2]. A limitation of discrete dislocation simulations is that they are applicable only for structures at the micrometer scale, since for larger systems they are computationally too expensive to be practical while they cannot resolve systems which are smaller than approximately a hundredth of a micrometer. For smaller scales, plasticity can be modeled by molecular dynamics simulations. Even though all these models are very helpful in understanding mechanics at a small scale, their validity as predictive tools is extremely limited.

Hence, there is the need for a comprehensive continuum plasticity theory which includes a material length scale. In the last twenty years many strain gradient plasticity theories have been formulated (see for reviews on the subject [3, 4]). Most of the non–local theories proposed [5]–[10] are based on a yield function that depends on gradients of the plastic strain. The mathematical formulation is quite different in the various models and discussion is still open about the order of the differential equations that should be involved in such a theory and the boundary conditions which should be applied. A common drawback of these non local theories is that the length scale(s) they incorporate are unknown material parameters, which need to be fitted to experimental results or to other independent models.

In this chapter the strain gradient theory proposed by Gurtin [11, 12, 13] for single crystals is discussed. The model is of particular interest in the content of this thesis since it focuses on the gradient effect caused by the net Burgers vector

*Based on *Effect of defect energy on strain gradient predictions of confined plasticity*, L. Nicola, E. van der Giessen, M. Gurtin, in preparation.

of dislocations. This single crystal plasticity theory is suitable for comparison with the results presented in chapter 1. The discrete dislocation results will be treated as numerical experimental data to fit the length scale appearing in Gurtin's theory. Different expressions for the defect energy in Gurtin's theory are proposed and discussed in this chapter. The aim is to see which ingredients are capable of capturing the size-dependent response of single crystalline films for different crystal orientations. The findings are aimed at assisting the further development of the theory.

6.1 Basic equations of Gurtin's theory

This theory [12] is meant to characterize single crystals undergoing plastic flow resulting from slip on specified slip systems. Attention is here confined to this theory for circumstances in which the material response is rate independent and geometry changes are negligible.

The theory is based on the standard crystalline decomposition

$$\boldsymbol{\nabla u} = \boldsymbol{H}^{\mathrm{e}} + \boldsymbol{H}^{\mathrm{p}}, \qquad \boldsymbol{H}^{\mathrm{p}} = \sum_{\beta} \gamma^{(\beta)} \mathbb{S}^{(\beta)} \tag{6.1}$$

of the dispacement gradient $\boldsymbol{\nabla u}$ into elastic and plastic parts, $\boldsymbol{H}^{\mathrm{e}}$ and $\boldsymbol{H}^{\mathrm{p}}$, where $\gamma^{(\beta)}$ represents the slip on slip system β. Here $\mathbb{S}^{(\beta)}$, the Schmid tensor for β, has the form

$$\mathbb{S}^{(\beta)} = \boldsymbol{s}^{(\beta)} \otimes \boldsymbol{m}^{(\beta)}, \qquad |\boldsymbol{s}^{(\beta)}| = |\boldsymbol{m}^{(\beta)}| = 1, \qquad \boldsymbol{s}^{(\beta)} \perp \boldsymbol{m}^{(\beta)}, \tag{6.2}$$

with $\boldsymbol{s}^{(\beta)}$ the slip direction and $\boldsymbol{m}^{(\beta)}$ the slip-plane normal.

The governing equations — derived from a formulation of the principle of virtual work that allows for microforce fields $\boldsymbol{\xi}^{(\beta)}$ and $\pi^{(\beta)}$ work-conjugate to slips $\boldsymbol{\gamma}^{(\beta)}$ and slip gradients $\boldsymbol{\nabla\gamma}^{(\beta)}$ — consist of the classical equilibrium condition

$$\operatorname{div} \boldsymbol{\sigma} = 0 \tag{6.3}$$

supplemented by the microforce balance

$$\operatorname{div}\boldsymbol{\xi}^{(\beta)} - \pi^{(\beta)} + \tau^{(\beta)} = 0, \qquad \tau^{(\beta)} = \mathbb{S}^{(\beta)} : \boldsymbol{\sigma}. \tag{6.4}$$

The requirement that the increase in free energy must be not greater than the rate of work leads to the free-energy inequality

$$\dot{\psi} - \boldsymbol{\sigma} : \dot{\boldsymbol{\varepsilon}}^{\mathrm{e}} - \sum_{\beta} (\boldsymbol{\xi}^{(\beta)} \cdot \boldsymbol{\nabla}\dot{\gamma}^{(\beta)} + \pi^{(\beta)} \dot{\gamma}^{(\beta)}) \leq 0, \tag{6.5}$$

where ψ is the free energy (per unit volume) and $\boldsymbol{\varepsilon}^{\mathrm{e}}$ is the elastic strain, the symmetric part of $\boldsymbol{H}^{\mathrm{e}}$. Here, in contrast to the classical crystalline theory, ψ is taken to have the additive form

$$\psi = \tfrac{1}{2}\boldsymbol{\varepsilon}^{\mathrm{e}} \cdot \boldsymbol{\mathcal{C}}\boldsymbol{\varepsilon}^{\mathrm{e}} + \Psi_{\mathrm{D}} \tag{6.6}$$

with strain-energy augmented by a defect energy Ψ_{D}, which we assume to be quadratic in the slip-gradients $\boldsymbol{\nabla}\gamma^{(\beta)}$. Here $\boldsymbol{\mathcal{C}}$ is the standard fourth-order tensor of elastic moduli, which, assuming isotropy, we express in terms of Young's modulus E and Poisson's ratio ν.

Guided by the classical theory and by the free-energy inequality (6.5), $\boldsymbol{\sigma}$, $\boldsymbol{\xi}^{(\beta)}$, and $\pi^{(\beta)}$ are presumed given by the constitutive equations

$$\boldsymbol{\sigma} = \boldsymbol{\mathcal{C}}\boldsymbol{\varepsilon}^{\mathrm{e}}\,, \qquad \boldsymbol{\xi}^{(\beta)} = \frac{\partial \Psi_{\mathrm{D}}}{\partial \boldsymbol{\nabla}\gamma^{(\beta)}}\,, \qquad \pi^{(\beta)} = \varphi^{(\beta)}\mathrm{sgn}\dot{\gamma}^{(\beta)}\,, \tag{6.7}$$

in which slip-system hardening, as described by the internal variables $\varphi^{(\beta)}$, is here taken to be local and isotropic:

$$\dot{\varphi}^{(\beta)} = \sum_{\kappa} H_0 |\dot{\gamma}^{(\kappa)}|\,, \qquad \varphi^{(\beta)}\Big|_{t=0} = \pi_0, \tag{6.8}$$

with π_0 the initial yield strength.

6.2 Macroscopic defect measures in plane strain

With a view toward comparison with two-dimensional discrete dislocation simulations, we henceforth restrict attention to plane strain, with deformation occurring in the (x_1, x_2) plane, so that $\boldsymbol{e}_3$ is the out-of-plane direction.

6.2.1 Burgers vector

The macroscopic Burgers vector is characterized by the Burgers tensor

$$\boldsymbol{G} = \mathrm{curl}\boldsymbol{H}^{\mathrm{p}} = \sum_{\beta} (\boldsymbol{\nabla}\gamma^{(\beta)} \times \boldsymbol{m}^{(\beta)}) \otimes \boldsymbol{s}^{(\beta)}, \tag{6.9}$$

but since we here restrict attention to plane strain, $\boldsymbol{G}$ has the simple form:

$$\boldsymbol{G} = \boldsymbol{e}_3 \otimes \boldsymbol{g}; \qquad \boldsymbol{g} = \sum_{\beta} \partial^{(\beta)}\gamma^{(\beta)}\boldsymbol{s}^{(\beta)}, \tag{6.10}$$

where for each slip system β, $\partial^{(\beta)}\Phi$ is the derivative in the direction of slip:

$$\partial^{(\beta)}\Phi = \boldsymbol{s}^{(\beta)} \cdot \boldsymbol{\nabla}\Phi. \tag{6.11}$$

Thus $\boldsymbol{G}$ may be viewed as representing an edge dislocation with Burgers vector $\boldsymbol{g}$ in the (x_1, x_2) plane and line direction $\boldsymbol{e}_3$. The Burgers vector resolved on slip system β has the form

$$\boldsymbol{g} \cdot \boldsymbol{s}^{(\beta)} = \sum_{\kappa} S^{(\beta\kappa)} \partial^{(\kappa)} \gamma^{(\kappa)}, \tag{6.12}$$

where $S^{(\beta\kappa)}$ are the slip-interaction coefficients

$$S^{(\beta\kappa)} = \boldsymbol{s}^{(\beta)} \cdot \boldsymbol{s}^{(\kappa)}. \tag{6.13}$$

6.2.2 Pile-up fields

We view $\partial^{(\beta)}\gamma^{(\beta)}$, the gradient of $\gamma^{(\beta)}$ in the direction of slip on β, as a macroscopic measure of the pile-up of dislocations on β.

For *double-slip* there is a one-to-one correspondence between the pile-up fields $\partial^{(\beta)}\gamma^{(\beta)}$ and the Burgers vector, since, by eq. (6.10),

$$\boldsymbol{g} \cdot \boldsymbol{m}^{(1)} = (\boldsymbol{m}^{(1)} \cdot \boldsymbol{s}^{(2)}) \partial^{(2)} \gamma^{(2)}, \qquad \boldsymbol{g} \cdot \boldsymbol{m}^{(2)} = (\boldsymbol{m}^{(2)} \cdot \boldsymbol{s}^{(1)}) \partial^{(1)} \gamma^{(1)}. \tag{6.14}$$

Because of this correspondence, the pile-ups can be expressed in terms of the slip-resolutions of the Burgers vector $\boldsymbol{g} \cdot \boldsymbol{s}^{(\beta)}$; in fact,

$$\left.\begin{aligned} \zeta^2 \partial^{(1)} \gamma^{(1)} &= \boldsymbol{g} \cdot \boldsymbol{s}^{(1)} - \mu \boldsymbol{g} \cdot \boldsymbol{s}^{(2)}, \\ \zeta^2 \partial^{(2)} \gamma^{(2)} &= \mu \boldsymbol{g} \cdot \boldsymbol{s}^{(1)} - \boldsymbol{g} \cdot \boldsymbol{s}^{(2)} \end{aligned}\right\} \tag{6.15}$$

with

$$\zeta = \boldsymbol{s}^{(1)} \cdot \boldsymbol{m}^{(2)}, \qquad \mu = \boldsymbol{m}^{(1)} \cdot \boldsymbol{m}^{(2)}.$$

When there are more than two slip systems there is no such correspondence: while the pile-ups determine the Burgers vector via (6.10), the Burgers vector cannot uniquely determine the pile-ups. In fact, it is possible that a set of pile-ups, not all zero, correspond to a null Burgers vector.

6.3 Defect energies

We now discuss various specific choices for the defect energy. Throughout this discussion the constant $\ell > 0$ represents a constitutive length scale.

6.3.1 Burgers-vector energies

We consider the following specific defect energies, here listed together with their associated microstresses:

(i) isotropic energy (cf. [12])

$$\Psi_{\mathrm{I}} = \tfrac{1}{2}\ell^2\pi_0|\boldsymbol{g}|^2, \qquad \boldsymbol{\xi}^{(\beta)} = \ell^2\pi_0\sum_{\kappa} S^{(\beta\kappa)}\partial^{(\kappa)}\gamma^{(\kappa)}\boldsymbol{s}^{(\beta)}; \tag{6.16}$$

(ii) energy dependent on the resolved values of the Burgers vector:

$$\begin{aligned}\Psi_{\mathrm{S}} &= \tfrac{1}{2}\ell^2\pi_0\sum_{\beta,\kappa} k^{(\beta\kappa)}(\boldsymbol{g}\cdot\boldsymbol{s}^{(\beta)})(\boldsymbol{g}\cdot\boldsymbol{s}^{(\kappa)}),\\ \boldsymbol{\xi}^{(\beta)} &= \ell^2\pi_0\textstyle\sum_{\phi,\kappa,\rho} S^{(\beta\phi)}k^{(\phi\kappa)}S^{(\kappa\rho)}\partial^{(\rho)}\gamma^{(\rho)}\boldsymbol{s}^{(\beta)},\end{aligned} \tag{6.17}$$

where

$$k^{(\beta\beta)} = 1 \quad \text{for all} \quad \beta, \qquad k^{(\beta\kappa)} = k, \quad \beta \neq \kappa, \tag{6.18}$$

with k a constant constitutive modulus. We also consider the special case in which $k = 0$, so that:

$$\Psi_{\mathrm{S0}} = \tfrac{1}{2}\ell^2\pi_0\sum_{\beta}(\boldsymbol{g}\cdot\boldsymbol{s}^{(\beta)})^2, \qquad \boldsymbol{\xi}^{(\beta)} = \ell^2\pi_0\sum_{\rho} S^{(\beta\phi)}S^{(\phi\rho)}\partial^{(\rho)}\gamma^{(\rho)}\boldsymbol{s}^{(\beta)}. \tag{6.19}$$

6.3.2 Pile-up energy

The pile-up energy and associated microstress have the form

$$\Psi_{\mathrm{P}} = \tfrac{1}{2}\ell^2\pi_0\sum_{\beta}(\partial^{(\beta)}\gamma^{(\beta)})^2, \qquad \boldsymbol{\xi}^{(\beta)} = \ell^2\pi_0\partial^{(\beta)}\gamma^{(\beta)}\boldsymbol{s}^{(\beta)}. \tag{6.20}$$

Unlike energies dependent on the Burgers vector, the microstress for the pile-up energy does not couple the individual slip systems.

For *double-slip*, we may use (6.15) to conclude that

$$\frac{\zeta^4}{1+\mu^2}\left[(\partial^{(1)}\gamma^{(1)})^2 + (\partial^{(2)}\gamma^{(2)})^2\right] = (\boldsymbol{g}\cdot\boldsymbol{s}^{(1)})^2 + (\boldsymbol{g}\cdot\boldsymbol{s}^{(2)})^2 - \frac{4\mu}{1+\mu^2}(\boldsymbol{g}\cdot\boldsymbol{s}^{(1)})(\boldsymbol{g}\cdot\boldsymbol{s}^{(2)}), \tag{6.21}$$

and hence that the pile-up energy is a special case of (6.17), albeit with a different π_0.

6.4 Summary of DD results for single crystal thin films on a substrate

The problem of a thin film on a semi-infinite substrate subjected to thermal loading as illustrated in Fig 6.1 has been studied using discrete dislocation (DD) simulations in [14] and [15].

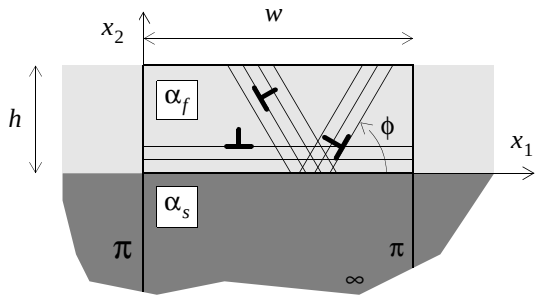

Figure 6.1 Geometry of the film-substrate problem studied in chapter 2. A unit cell of width w is analyzed and the height of the substrate is taken large enough to represent a half space.

A quasi-static monotonic thermal loading is imposed by cooling the film–substrate system from an initial temperature T_0, at which film and substrate are stress–free and dislocation–free. The substrate undergoes unconstrained contraction but, due to the mismatch between the thermal expansion coefficient of film (α_f) and substrate (α_s), stress develops in the film; tensile for $\alpha_f > \alpha_s$. After an initial elastic response, dislocations nucleate in the film and partially relax the stress in the film by gliding on three sets of parallel slip planes. We focus on two crystal orientations: $\phi_{60} = (0^\circ, 60^\circ, 120^\circ)$ and $\phi_{30} = (30^\circ, 90^\circ, 150^\circ)$.

Results obtained for three different film thicknesses —$h = 1\mu$m, $h = 0.5\mu$m and $h = 0.25\mu$m— show that the average in-plane stress in the films is dependent on the film thickness. Results also show that hardening depends on crystal orientation: relaxation in films with orientation ϕ_{30} is higher than in films with slip planes oriented ϕ_{60}. Moreover, the size effect is more evident for the ϕ_{60} orientation.

In both crystal orientations, the size dependence originates from the large stress gradient at the film-substrate interface, caused by dislocation pile ups. Instead of a uniform stress distribution across the film height, as in the elastic state or accord-

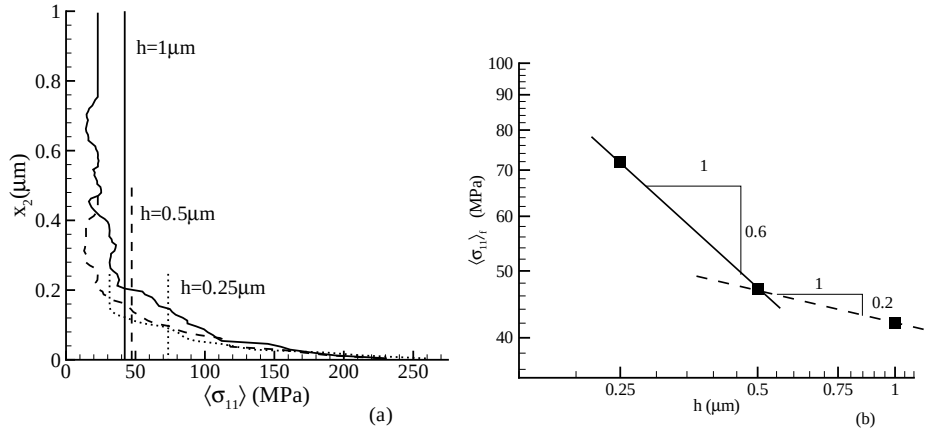

Figure 6.2 DD results [14] after cooling by 200K for the crystal orientation ϕ_{30}. (a) Profiles across the film thickness of the in-plane stress in the films averaged along x_1. (b) Average film stress versus film thickness: data points are fitted to a power law of the form $\langle\sigma_{11}\rangle_{\mathrm{f}} \propto h^{-p}$.

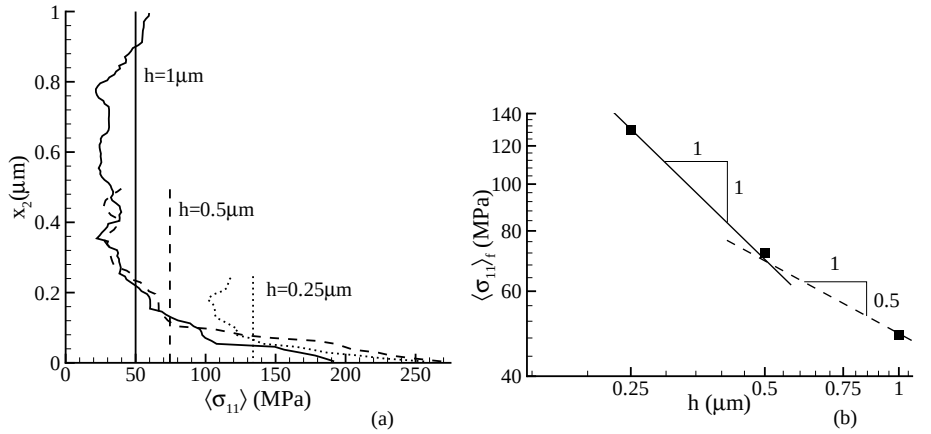

Figure 6.3 DD results [14] for ϕ_{60}. (a) Profiles across the film thickness of the in-plane stress in the films averaged along x_1. (b) Average film stress versus film thickness with data points being fitted to a power law of the form $\langle\sigma_{11}\rangle_{\mathrm{f}} \propto h^{-p}$.

ing to classical local plasticity, the stress increases as the interface is approached, see Fig. 6.2a for ϕ_{30} and see Fig. 6.3a for ϕ_{60}. The vertical lines in these figures indicate the average stress in each film, $\langle\sigma_{11}\rangle_{\mathrm{f}}$. This data is tentatively fitted in Figs. 6.2b and 6.3b to power laws of the form $\sigma_{11} \propto h^{-p}$. Since different values of

p are needed to fit the data, such kind of a power law appears not to be appropriate.

6.5 Closed-form solution of the thin film problem

We simplify the three-slip system model used in the DD simulations (Fig. 6.1) to one with only two slip systems. In the ϕ_{60} orientation, the slip plane parallel

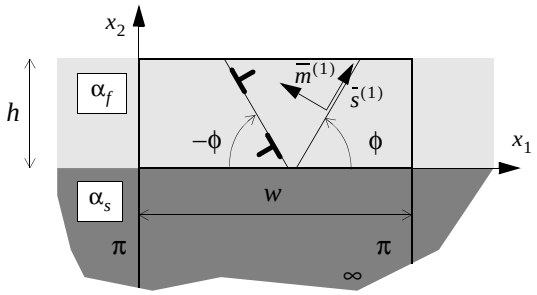

Figure 6.4 Geometry of the thin film problem in symmetric double slip.

to the interface is hardly active and is therefore ignored. For the same reason, the 90° slip plane in the ϕ_{30} orientation is not considered in the application of the continuum theory. Thus, we consider the crystal to be oriented for symmetric double slip with the angle $\phi^{(\beta)}$ between slip plane and film–substrate interface being $\phi^{(1)} \equiv \phi$ and $\phi^{(2)} = \pi - \phi$. Then

$$\boldsymbol{s}^{(1)} = \cos\phi\boldsymbol{e}_1 + \sin\phi\boldsymbol{e}_2\ ,\ \boldsymbol{m}^{(1)} = -\sin\phi\boldsymbol{e}_1 + \cos\phi\boldsymbol{e}_2\ ; \tag{6.22}$$

$$\boldsymbol{s}^{(2)} = -\cos\phi\boldsymbol{e}_1 + \sin\phi\boldsymbol{e}_2\ ,\ \boldsymbol{m}^{(2)} = -\sin\phi\boldsymbol{e}_1 - \cos\phi\boldsymbol{e}_2 \tag{6.23}$$

The macroscopic boundary conditions prescribed are the traction-free conditions at the top of the film:

$$\sigma_{12}(x_1,h) = \sigma_{22}(x_1,h) = 0\,. \tag{6.24}$$

The additional, microscopic boundary conditions are the micro-free condition at the film top, where dislocations can freely leave the film, and the micro-clamped condition at the film–substrate interface where slip cannot occur, i.e.

$$n_i\xi_i^{(\beta)}(x_1,h) = \xi_2^{(\beta)}(x_1,h) = 0\,, \qquad \gamma^{(\beta)}(x_1,0) = 0\,. \tag{6.25}$$

Since the film is infinitely long in the x_1-direction and initially homogeneous, the solution depends only on x_2. With all stress components independent of x_1,

equilibrium together with the macroscopic boundary conditions (6.24) requires that $\sigma_{12} = \sigma_{22} = 0$ throughout the film. The elastic solution is a spatially uniform field $\sigma_{11}(x_2) = \text{const}$, so that yield takes place uniformly in the crystal when $\tau^{(\beta)} = |\pi_0|$ on both slip systems, with

$$\tau^{(1)} = -\tau^{(2)} = -\tfrac{1}{2}\sigma_{11}\sin 2\phi \equiv -\tau. \tag{6.26}$$

Because of the double slip orientation and symmetry,

$$\gamma^{(1)} = -\gamma^{(2)} \equiv -\gamma, \tag{6.27}$$

where it is expected that $\gamma \geq 0$ since $\tau \geq 0$ for the orientations studied here.

Owing to (6.27), the yield conditions on the two slip systems lead to the same differential equation for $\gamma(x_2)$. The time derivative of this equation can be expressed as:

(i) for the isotropic energy, eq. (6.16)

$$\frac{d^2\dot{\gamma}}{dx_2^2} = -\frac{\dot{\sigma}_{11}}{\ell^2\pi_0\sin 2\phi}; \tag{6.28}$$

(ii) for the Ψ_{S0} energy, eq. (6.19)

$$\frac{d^2\dot{\gamma}}{dx_2^2} = -\frac{\dot{\sigma}_{11}}{\ell^2\pi_0 2\sin 2\phi\cos^2\phi}; \tag{6.29}$$

(iii) for the Ψ_S energy, eq. (6.17)

$$\frac{d^2\dot{\gamma}}{dx_2^2} = -\frac{\dot{\sigma}_{11}}{(1-k)\ell^2\pi_0 2\sin 2\phi\cos^2\phi}; \tag{6.30}$$

(iv) for the pile-up energy, eq. (6.20)

$$\frac{d^2\dot{\gamma}}{dx_2^2} = -\frac{\dot{\sigma}_{11}\cot\phi}{\ell^2\pi_0}. \tag{6.31}$$

The stress field $\sigma_{11}(x_2)$ is not uniform and unknown at this stage. Because of symmetry and because strain rate components do not depend on x_1, $\dot{\varepsilon}_{11}$ must be uniform throughout the film. The stress field can be determined by ensuring that this is the case. The total strain splits up into an elastic part, a plastic part and a thermal part given by $\varepsilon_{ij}^T = (1+\nu)\alpha\Delta T\delta_{ij}$ ($(1+\nu)$ stems from the plane

strain formulation). Considering that the substrate expands by $\varepsilon_{11} = (1+\nu)\alpha_s \dot{T}$, compatibility of deformation between the film and the substrate requires that $\dot{\varepsilon}_{11}$ is the same and uniform throughout the film. Hence,

$$(1+\nu)\alpha_s \dot{T} = \dot{\varepsilon}^e_{11} + \dot{\varepsilon}^p_{11} + (1+\nu)\alpha_f \dot{T} \tag{6.32}$$

so that

$$(1+\nu)(\alpha_s - \alpha_f)\dot{T} = \frac{(1-\nu^2)}{E}\dot{\sigma}_{11} + \dot{\gamma}\sin 2\phi\,. \tag{6.33}$$

Eliminating $\dot{\sigma}_{11}$ by means of (6.28), we obtain the following ordinary second-order differential equation for $\dot{\gamma}$:

$$\frac{d^2\dot{\gamma}}{dx_2^2} - \lambda^2\dot{\gamma} = -F \tag{6.34}$$

with constant coefficients λ and F given through

$$\lambda^2 = \frac{E}{(1-\nu^2)\ell^2\pi_0 f(\phi)}\,, \qquad F = \frac{E(\alpha_s - \alpha_f)\dot{T}}{(1-\nu)\ell^2\pi_0 \sin 2\phi\, f(\phi)}\,. \tag{6.35}$$

Here, $f(\phi)$ is a function of orientation ϕ which, depending on the energy considered, takes the following forms:

(i) for the isotropic energy, eq. (6.16)

$$f(\phi) = 1 \tag{6.36}$$

(ii) for the Ψ_{S0} energy, eq. (6.19)

$$f(\phi) = 2\cos^2\phi \tag{6.37}$$

(iii) for the Ψ_S energy, eq. (6.17)

$$f(\phi) = (1-k)2\cos^2\phi \tag{6.38}$$

(iv) for the pile-up energy, eq. (6.20)

$$f(\phi) = \frac{1}{2\cos^2\phi}\,. \tag{6.39}$$

Dependence on the dissipative hardening modulus H_0 was found to be so weak that the solution is here given for $H_0 = 0$. Solving eq. (6.34) subject to the microscopic boundary conditions (6.25) and (6.26) we obtain the solution

$$\dot{\gamma} = \frac{F}{\lambda^2}[1 - \cosh\lambda x_2 + \tanh\lambda h \sinh\lambda x_2], \tag{6.40}$$

where for all energies

$$\frac{F}{\lambda^2} = \frac{(1+\nu)(\alpha_s - \alpha_f)\dot{T}}{\sin 2\phi}. \tag{6.41}$$

Substituting equation (6.40) back into (6.33), we find a linear relation between $\dot{\sigma}_{11}$ and $\dot{T}$, which, after integration from the onset of yield (at temperature $T_y < T_0$) to the current temperature T, gives

$$\sigma_{11} = \sigma_y + (\sigma_n - \sigma_y)[\cosh\lambda x_2 - \tanh\lambda h \sinh\lambda x_2]. \tag{6.42}$$

Here,

$$\sigma_y = -\frac{E}{1-\nu}(\alpha_f - \alpha_s)(T_y - T_0), \qquad \sigma_n = -\frac{E}{1-\nu}(\alpha_f - \alpha_s)(T - T_0) \tag{6.43}$$

are the (uniform) film stress at the onset of yield (at temperature T_y) and the stress in the absence of plasticity, respectively. The solutions for the different defect energies differ only through the ϕ-dependence of λ.

6.6 Comparison of the non-local theory with DD simulations

6.6.1 The isotropic energy

The closed-form expression for the stress distribution (6.42) can readily be integrated over the film thickness to give the film-average stress as a function of h. Evidently, the solution depends on the values of four material parameters: E, ν, π_0 and ℓ. For the elastic constants we take the same characteristic values for aluminum ($E = 70$GPa and $\nu = 0.33$) as in the DD simulations presented in Sec. 6.4. The initial shear strength π_0 is taken from the DD results to be $\pi_0 = 15.5$MPa, corresponding to a film stress of $4/\sqrt{3}\pi_0 = 36$MPa [14]. Yield in the DD simulations is determined by the strength of the weakest dislocation source. The values of the source strengths in the simulations were chosen out of a Gaussian distribution with average $\tau_{nuc} = 25$MPa and standard deviation of 5MPa.

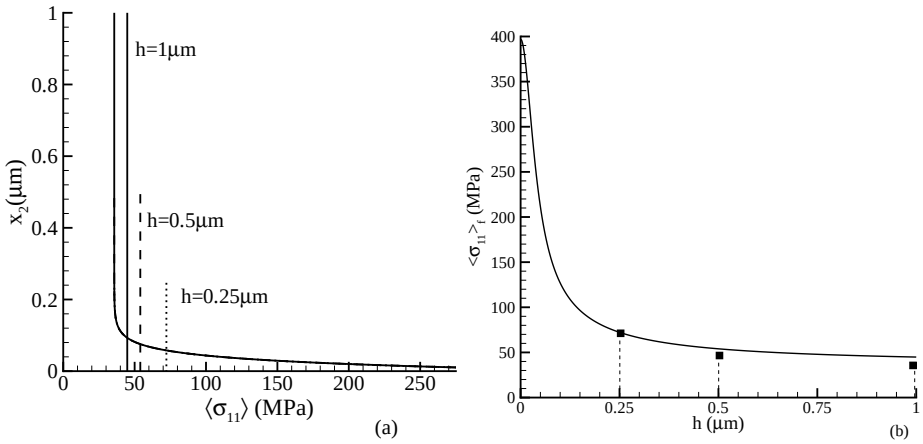

Figure 6.5 Predictions according to the isotropic defect energy theory, eq. (6.16), for $\phi = 30^\circ$ with $\ell = 1.8\mu$m at the same final temperature as in Fig. 6.2. (a) Profiles of the in-plane stress across the film thickness. Vertical lines indicate the average stress in the films, which are plotted in (b) as a function of film thickness h (scaling behavior $\langle\sigma_{11}\rangle_f \propto \tanh\lambda h/\lambda h$). Square symbols indicate the data points from the DD simulations.

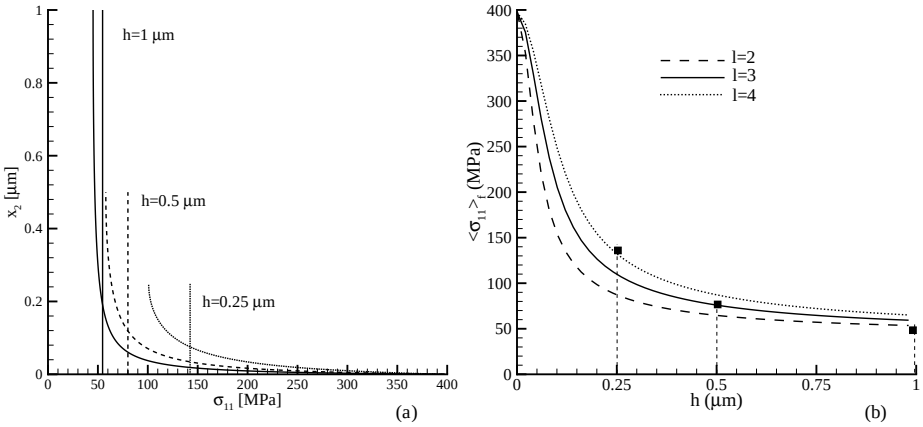

Figure 6.6 Predictions according to the isotropic defect energy theory, eq. (6.16), for $\phi = 60^\circ$ at the same final temperature as in Fig. 6.3. (a) Profiles of the in-plane stress across the film thickness with $\ell = 1.8\mu$m. (b) The average film stress as a function of film thickness h for three values of ℓ: $\ell = 2$, 3 and 4μm. Square symbols indicate the data points from the DD simulations.

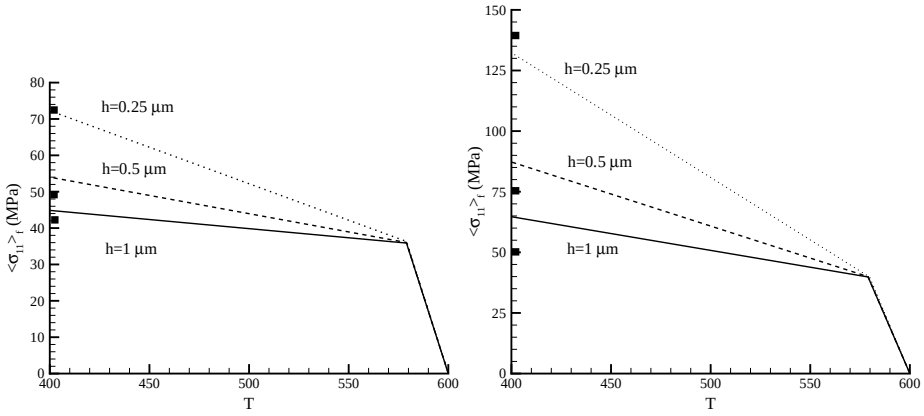

Figure 6.7 Film-average stress-temperature curves according to the strain gradient solution eq. (6.42) according to the isotropic defect energy theory, eq. (6.16), for (a) $\phi = 30^\circ$ with $\ell = 1.8\mu$m and (b) for $\phi = 60^\circ$ with $\ell = 4\mu$m. Square symbols indicate the stress at final temperature in the DD simulations, as shown also in Figs. 6.2, 6.5 and Figs. 6.3, 6.6.

The only parameter left free is the length scale ℓ originating from (6.16). It is clear from eq (6.42) that the DD results for the two crystal orientations cannot be fitted using a single value of the material parameter ℓ: the equation depends on ϕ only through $\sin 2\phi$, which is the same number for $\phi = 60^\circ$ and $\phi = 30^\circ$. A value of $\ell = 1.8\mu$m gives a $\langle\sigma_{11}\rangle_f$–$h$ curve which agrees quite well with the DD data points in the case of ϕ_{30}, as shown in Fig. 6.5b. We tried, without success, to find a value of ℓ giving a similar fit to the $\langle\sigma_{11}\rangle_f$–$h$ dislocation data for the slip plane orientation with ϕ_{60}. Figure 6.6b shows three curves for $\ell = 2$, 3 and 4μm, each of them agreeing only with the DD data for a single particular thickness h. Figures 6.5a and 6.6a show the stress profiles across the film height according to (6.42), which indeed exhibit a stress gradient. Another noteworthy feature of the solution is that the stress at the film–substrate interface is independent of h, and equal to the elastic stress σ_n, eq. (6.43). Figure 6.7, finally, shows the stress–temperature curves given by the solution (6.42), which reinforces the difficulties in obtaining a good fit for ϕ_{60}.

6.6.2 The S0 Defect Energy

The solution for this theory, with $f(\phi)$ according to (6.37), also has only the length scale ℓ as a free material parameter. For $\ell = 1.5\mu$m it is possible to fit the DD

results for the ϕ_{30} orientation, but the solution for the same material length scale for the orientation ϕ_{60} does not match the DD results. The curves in Fig. 6.8 show an opposite trend with respect to the DD predictions: the size effect is smaller for the ϕ_{60} orientation than for the ϕ_{30}.

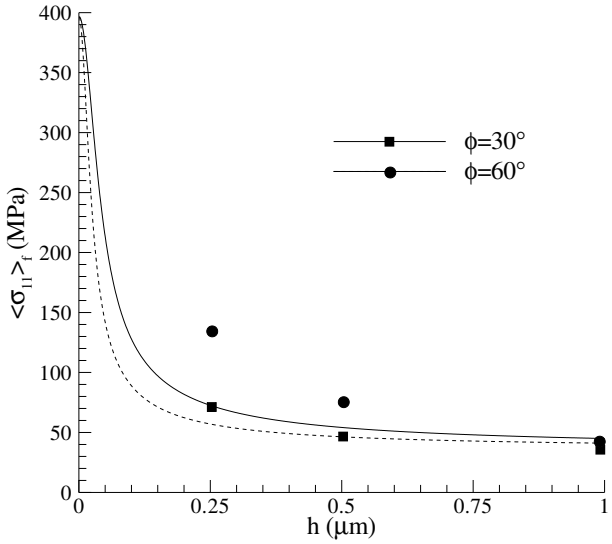

Figure 6.8 Average stress in the films versus film thickness *h* predicted by the S0 defect energy theory, eq. (6.19), for $\phi = 30^\circ$ and $\phi = 60^\circ$. The symbols represent the discrete dislocation results.

6.6.3 The S Defect Energy

In this case, with $f(\phi)$ according to (6.38), there is an additional free parameter, *k*, beside the material length scale ℓ. This allows for a good fit of the two orientations, provided that *k* is different for the ϕ_{30} and for the ϕ_{60} orientation. In particular, *k* must be positive for the ϕ_{30} orientation, negative for the ϕ_{60}. Figure 6.9 shows the fit obtained for $\ell = 3\mu$m.

6.6.4 The Pile-up Defect Energy

By considering the free energy in the form of the pile-up defect energy, eq. (6.20), we again have only one free material parameter for the fit with the simulations, ℓ. Even though the fit shown in Fig. 6.10 is not as good as the one obtained for the

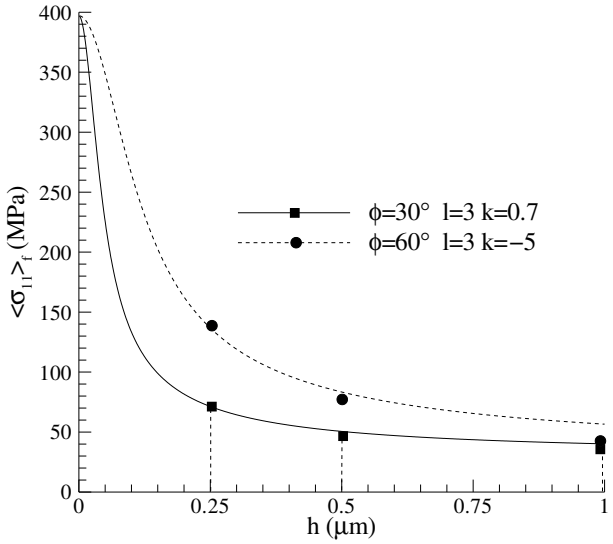

Figure 6.9 Film-average tensile stress as a function of film thickness *h* for two orientations according to the S-theory.

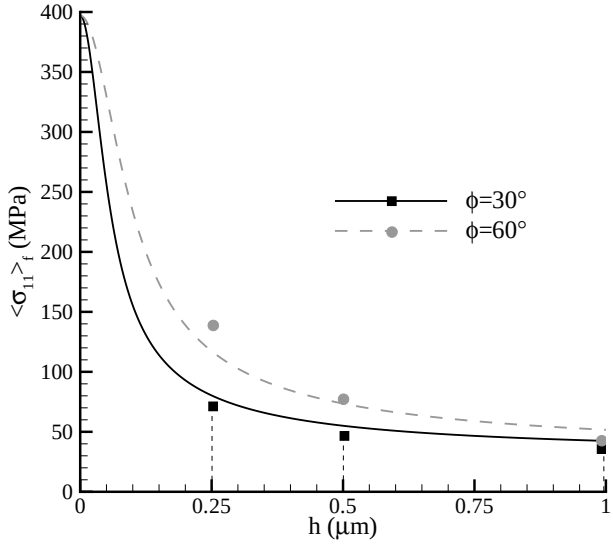

Figure 6.10 Film-average tensile stress as a function of film thickness *h* for two orientations according to the pile-up theory.

S-energy, there still is a quite good agreement for $\ell = 3\mu$m. It is worth noticing that the S-energy reduces to the S0-energy for $k = 0$, to the pile-up energy for $k = 1 - 1/4\cos^2\phi$ ($k_{30} = 0.\overline{5}$, $k_{60} = -3$).

6.7 Conclusions

Different forms for the free energy in Gurtin's strain gradient plasticity theory have been discussed. The problem of a thin film strained by a large substrate during cooling has been solved by discrete dislocation plasticity simulations and by the strain gradient theory, using different expressions for the free energy. The best fit between simulations and theory has been found for a defect energy in the form of a pile-up energy.

References

[1] H.H.M. Cleveringa, Discrete Dislocation Plasticity, PhD Thesis, ISBN 90-423-0091-4.

[2] H.H.M. Cleveringa, E. Van der Giessen, A. Needleman, Acta Mater. **45** (1997) 3143.

[3] J.W. Hutchinson, Int. J. Solid Struct **37** (2000) 225.

[4] A. Needleman, Acta Mater. **48** (2000) 105.

[5] E.C. Aifantis, Int. J. Eng. Sci. **30** (1992) 1279.

[6] E.C. Aifantis, Int. J. Frac. **95** (1999) 299.

[7] N.A. Fleck, J.W. Hutchinson, Adv. Appl. Mech. **33** (1997) 295.

[8] N.A. Fleck, J.W. Hutchinson, J. Mech. Phys. Solids **49** (2001) 2245.

[9] J.L. Bassani, J. Mech. Phys. Solids **49** (2001) 1983.

[10] Y. Huang, H. Gao, W.D. Nix, J.W. Hutchinson, J. Mech. Phys. Solids, **48** (2000) 99.

[11] M.E. Gurtin, J. Mech. Phys. Solids **48** (2000) 989.

[12] M.E. Gurtin, J. Mech. Phys. Solids **50** (2002) 5.

[13] M.E. Gurtin, Int. J. Plast. **19** (2003) 47.

[14] L. Nicola, E. van der Giessen and A. Needleman, J. Appl. Phys **93** (2003) 5920.

[15] L. Nicola, E. van der Giessen, A. Needleman, submitted for publication.